Effect of classical bifurcations on the quantum entanglement of two coupled quartic oscillators

M. S. Santhanam,[1] V. B. Sheorey,[1] and Arul Lakshminarayan[2,*]
[1]*Physical Research Laboratory, Navrangpura, Ahmedabad 380009, India*
[2]*Max Planck Institute for the Physics of Complex Systems, Nöthnitzer Strasse 38, Dresden 01187, Germany*
(Received 6 July 2007; revised manuscript received 8 October 2007; published 19 February 2008)

We study entanglement in a system comprising two coupled quartic oscillators. It is shown that the entanglement, as measured by the von Neumann entropy, increases with the classical chaos parameter for generic chaotic eigenstates. We consider certain isolated periodic orbits whose bifurcation sequence affects a class of strongly scarred quantum eigenstates, called the channel localized states. For these states, the entanglement is a local minima in the vicinity of a pitchfork bifurcation but is a local maxima near an antipitchfork bifurcation. We place these results in the context of the close connections that may exist between entanglement measures and conventional measures of localization. We also point to an interesting near degeneracy that arises in the spectrum of reduced density matrices of certain states as an interplay between localization and symmetry.

DOI: 10.1103/PhysRevE.77.026213 PACS number(s): 05.45.Mt, 03.67.Mn

I. INTRODUCTION

Quantum entanglement is currently an active area of research as it is a physical resource for tasks of quantum information processing such as quantum computing, quantum cryptography, and teleportation [1]. Although entanglement does not have a classical counterpart, it is being increasingly realized that the nature of classical dynamics, such as whether it is regular or chaotic, affects entanglement in the quantized system [2]. In general, larger chaos in the system leads to greater entanglement production, especially of the multipartite kind. This has been established by considering kicked top models [3], bakers map [4], Dicke model [5], billiards in magnetic fields [6], kicked Bose-Einstein condensates [7], and *N*-atom Jaynes-Cummings model [8]. In contrast to these studies, the role of classical bifurcations on entanglement has not received much attention. Apart from the gross increase of entanglement due to the presence of chaos, individual orbit bifurcations can also affect entanglement of quantum states that are influenced by these orbits in a semiclassical sense.

For instance, ions driven by laser fields and coupled to a heat bath, described by a form of Dicke model was shown to exhibit maximal entanglement of its ground state at the parameter value at which the classical system shows a bifurcation in phase space [9]. The ground state entanglement of the monomode Dicke model is shown to be related to Hopf bifurcation [10]. A similar result for the ground state was reported from the study of coupled tops, which itself is a generalization of the two-dimensional transverse field quantum Ising model [11] as well as for the Jahn-Teller models [12]. Qualitatively similar results for two component Bose-Einstein condensate are also known [13]. In all these cases, the treatment is confined mostly to the ground state of the system that exhibits criticality and involves one single classical bifurcation.

As opposed to a single bifurcation, what happens in bifurcation sequences where stability loss and stability gain interleave one another? What happens when bifurcations take place in the typical setting of a chaotic phase space? Both these questions explore the connection between chaos and entanglement in a physical setting that is different from those of earlier studies. In this context, we examine a Hamiltonian system whose classical dynamics is controlled by a single parameter, whose variation lead to a transition from integrability to chaos and bifurcation sequences of orbits that strongly scar quantum states. Consider, for instance, coupled nonlinear oscillator systems, a paradigm of chaos in smooth Hamiltonian systems and related to atoms in strong magnetic fields, viz., the quadratic Zeeman effect problems [14]. In these cases, one particular sequence of bifurcations is a series of pitchfork and antipitchfork bifurcations [15]. The pitchfork corresponds to a periodic orbit losing stability and in the Poincaré section this appears as an elliptic fixed point giving way to a hyperbolic fixed point. The antipitchfork is when the periodic orbit gains stability. In this work, we consider coupled quartic oscillators and show that the entanglement in a class of highly excited states of the system is modulated by classical bifurcations. Further, we place this in the context of investigations that lend support to the notion, that for generic one-particle states there is a strong correlation between entanglement and measures of localization [16–18].

II. ENTANGLEMENT IN A BIPARTITE SYSTEM

A pure quantum state $|\Psi\rangle$ composed of many subsystems $|\phi_i\rangle$ is said to be entangled if it cannot be written as a direct product of states corresponding to the subsystem

$$|\Psi\rangle_{\text{entangled}} \neq |\phi_1\rangle \otimes |\phi_2\rangle \otimes |\phi_3\rangle \cdots \otimes |\phi_n\rangle. \tag{1}$$

Thus, entanglement implies stronger than classical correlations. If $\rho=|\psi\rangle\langle\psi|$ is the density matrix representation for a pure state $|\psi\rangle$, then the reduced density matrix (RDM) can be obtained by applying the trace operation to one of the degrees of freedom. Thus,

$$\rho_1 = \mathrm{Tr}_2|\psi\rangle\langle\psi|, \quad \rho_2 = \mathrm{Tr}_1|\psi\rangle\langle\psi| \tag{2}$$

are two RDMs, where one of the degrees of freedom is traced out. The notation Tr_i denotes that the trace operation is

*Permanent address: Department of Physics, Indian Institute of Technology Madras, Chennai, 600036, India.

applied to the ith degree of freedom. Schmidt decomposition [1] provides an optimal representation for $|\psi\rangle$ in terms of product basis states,

$$|\psi\rangle = \sum_{i=1}^{N} \sqrt{\lambda_i} |\phi_i\rangle_{(1)} |\phi_i\rangle_{(2)}, \tag{3}$$

where $|\phi_i\rangle_{(1)}$ and $|\phi_i\rangle_{(2)}$ are the eigenvectors of the RDMs ρ_1 and ρ_2, respectively, and λ_i are the eigenvalues of either of the RDMs. The entanglement content of the pure state $|\psi\rangle$ is given by von Neumann entropy of the RDMs,

$$S = -\sum_{i=1}^{N} \lambda_i \ln \lambda_i. \tag{4}$$

Thus, when $S=0$, the state $|\psi\rangle$ is not entangled and when $S>0$, it is. The Schmidt decomposition provides a compact and unique representation for the given eigenstate (unique in the generic case when the nonzero spectrum of the RDM is nondegenerate).

III. HAMILTONIAN AND BIFURCATION SEQUENCE

A. Coupled quartic oscillators

We consider the Hamiltonian system given by

$$H = p_x^2 + p_y^2 + x^4 + y^4 + \alpha x^2 y^2 \tag{5}$$

with α being the chaos parameter. For $\alpha=0,2,6$, the system is classically integrable and becomes predominantly chaotic as $\alpha \to \infty$. This has been extensively studied as a model for classical and quantum chaos in smooth Hamiltonian systems [19] and exhibits dynamics that are qualitatively similar to problems involving Rydberg atoms in external fields. The limit $\alpha \to \infty$ is also of relevance as a model for classical Yang-Mills field theory [20]. To study the quantum analog of this system, we quantize it in a symmetrized basis set given by

$$\psi_{j(n_1,n_2)}(x,y) = \mathcal{N}[\phi_{n_1}(x)\phi_{n_2}(y) + \phi_{n_2}(x)\phi_{n_1}(y)], \tag{6}$$

where $\mathcal{N}=\mathcal{N}(n_1,n_2)$ is the normalization constant and $\phi(x)\phi(y)$ is the eigenstate of the unperturbed quartic oscillator with $\alpha=0$. The choice of this form of basis set is dictated by the fact that the quartic oscillator has C_{4v} point group symmetry, i.e., all the invariant transformations of a square. Hence, we have chosen the symmetry adapted basis sets as in Eq. (6) from A_1 representation of the C_{4v} point group.

Thus, the nth eigenstate is

$$\Psi_n(x,y) = \sum_{j(n_1,n_2)=1} a_{n,j(n_1,n_2)} \psi_{n_1,n_2}(x,y), \tag{7}$$

where $a_{n,j(n_1,n_2)}=\langle \psi(x,y) | \Psi_n(x,y) \rangle$ are the expansion coefficients in the unperturbed basis space. The integer j is the index for the basis state such that a one-to-one mapping between j and (n_1,n_2) exists. Note that n_1,n_2 are even integers and $a_{n,j(n_1,n_2)}=a_{n,j(n_2,n_1)}$ in the A_1 representation of the C_{4v} point group. In our calculations, we use m one-dimensional even parity states, i.e., $n_1,n_2=0,2,4,6,\ldots,m$ and we truncate at $m=318$. This leads to $j=1,2,3,\ldots,12\,880$ basis states for the problem. Thus, the eigenvalue equation is solved numerically by setting up Hamiltonian matrices of dimension 12 880 using $M=(m+2)/2=160$ one-dimensional basis states.

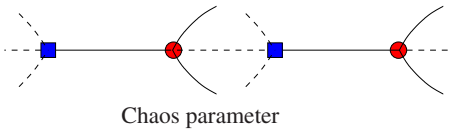

FIG. 1. (Color online) The schematic of a typical bifurcation sequence involving a series of pitchfork (circles) and antipitchfork (square) bifurcations as a function of chaos parameter. The solid line indicates that the orbit is stable and the dashed line indicates instability.

B. Bifurcation sequence in the coupled quartic oscillator

In general, a chaotic system may exhibit several bifurcation sequences. However, a two-dimensional Hamiltonian system can exhibit five and only five types of bifurcations [15]. One such prominent sequence is a series of pitchfork and antipitchfork bifurcation shown schematically in Fig. 1. To reiterate, a pitchfork bifurcation takes place when a stable orbit loses its stability and gives birth to two stable orbits. Antipitchfork bifurcations occur when a stable orbit is spontaneously born due to the merger of two unstable orbits. We will focus on a particular periodic orbit, referred to as the channel orbit in the literature [21], given by the initial conditions $\{x,y=0,\ p_x,p_y=0\}$, which displays such a bifurcation sequence. The Poincaré section in the vicinity of the channel orbit has interesting scaling properties and the orbit itself has profound influence on a series of quantum eigenstates, called localized states, in the form of density enhancements or scars [22]. Such density enhancements due to channel orbits have also been noted in atoms in strong magnetic fields, i.e., the diamagnetic Kepler problem [23].

The stability of the channel orbit in the quartic oscillator in Eq. (5) is indicated by the trace of the monodromy matrix $J(\alpha)$ obtained from linear stability analysis. For the channel orbits, it is analytically obtained as [24]

$$\mathrm{Tr}\, J(\alpha) = 2\sqrt{2} \cos\left(\frac{\pi}{4}\sqrt{1+4\alpha}\right). \tag{8}$$

The channel orbit is stable provided $|\mathrm{Tr}\, J(\alpha)|<2$ and it undergoes bifurcations whenever $\mathrm{Tr}\, J(\alpha)=\pm 2$. From this condition, it is clear that the bifurcations take place at $\alpha_n=n(n+1)$ $(n=1,2,3,\ldots)$. Thus the channel orbit undergoes denumerably infinite number of pitchfork and antipitchfork bifurcations at $\alpha=\alpha_n$. Note that for $n=9$, we have $\alpha=90$ as one of the pitchfork bifurcation points. The Poincaré sections displayed in Fig. 2 shows that the stable channel orbit at $\alpha=90$ [Fig. 2(a)] bifurcates and gives birth to two new stable orbits [Fig. 2(b)] while the channel orbit itself becomes unstable. Thus, pitchfork bifurcations take place at $\alpha_n=2,12,30,56,90,\ldots$ and antipitchfork at $\alpha_n=6,20,42,72,\ldots$. This can be clearly observed from the plot of $\mathrm{Tr}\, J(\alpha)$ as a function of α shown in Fig. 3.

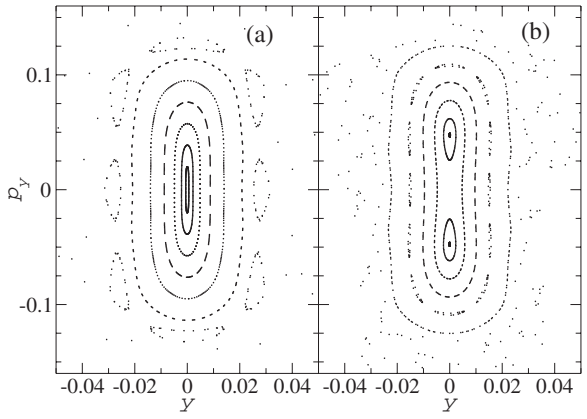

FIG. 2. The Poincaré section in the vicinity of the channel orbit for the quartic oscillator in Eq. (5) shown for (a) $\alpha=90$ and (b) $\alpha=90.5$. Note that at $\alpha=90$ this periodic orbit undergoes a pitchfork bifurcation.

IV. COUPLED QUARTIC OSCILLATOR STATES AND THEIR REDUCED DENSITY MATRIX

A. Coupled quartic oscillator spectra

The quantum spectrum of the quartic oscillator is extensively studied and reported [19,22,25]. For the purposes of this study, we note that two classes of eigenstates can be identified. The first one is what we call a generic state whose probability density $|\Psi_n(x,y)|^2$ covers the entire accessible configuration space. Most of the eigenstates fall in this class and they are instances of Berry's hypothesis that the Wigner function of a typical chaotic state condenses on the energy shell [26]. In Fig. 4(a), we show the expansion coefficients for the 1973rd eigenstate of the quartic oscillator counted sequentially from the ground state for $\alpha=90$. Notice that the state is delocalized over a large set of basis states. These classes of states are well described by random matrix theory. All channel localized states belong to the other class of strongly scarred states. These have enhanced probability density in the vicinity of the underlying channel periodic orbits. Theoretical underpinning for such density enhancements is based on semiclassical arguments of Heller [27], and of

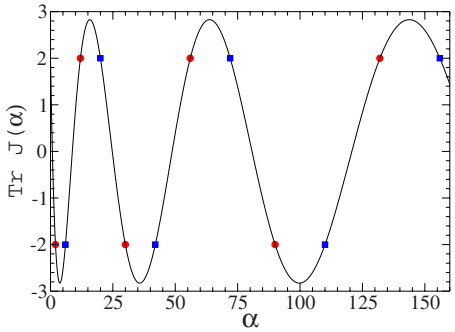

FIG. 3. (Color online) The linear stability of the channel orbit as a function of α. The orbit is stable for $|\mathrm{Tr}\, J(\alpha)|<2$. The pitchfork bifurcation points are indicated by circles and antipitchfork bifurcations are indicated by squares.

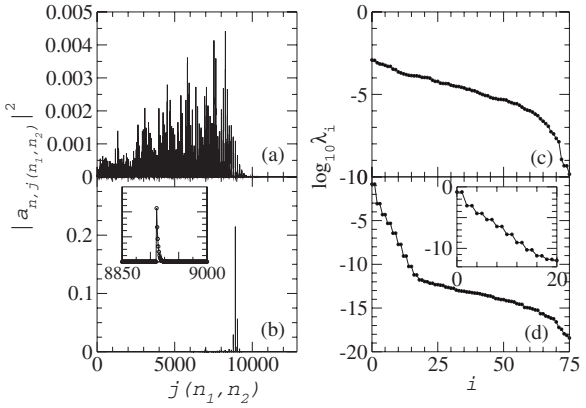

FIG. 4. Quartic oscillator eigenstates for $\alpha=90$ in the unperturbed basis. (a) The 1973rd state (delocalized), (b) the 1972nd state (localized). The inset is the magnification of the dominant peak. The eigenvalues of the RDMs for (c) the 1973rd state and (d) the 1972nd state. The inset in (d) is the magnification of the dominant eigenvalues that display degeneracy.

Bogomolny and Berry [28]. As a typical case, Fig. 4(b) shows the expansion coefficients for the 1972nd state which is localized over very few basis states in contrast to the one in Fig. 4(a). In this work, we concentrate on this subset of such eigenstates whose probability density is concentrated in the vicinity of the channel periodic orbit. This set of states are almost separable and can be approximately labeled by a doublet of quantum numbers $(N,0)$ using the framework of adiabatic theory [22,25]. Note that such a labeling is not possible for the generic states since they are spread over a large number of basis states and are therefore considered chaotic.

B. Reduced density matrix

In this section, we compute the eigenvalues of the RDM and the entanglement entropy of the quartic oscillator eigenstates as a function of the chaos parameter α. In terms of the expansion coefficients in Eq. (7), the elements of the RDM, $\mathbf{R}_x$, can be written as

$$\langle n_2|\rho^{(x)}|n_2'\rangle = \sum_{n_1=0}^{m} K_{n_1,n_2} a_{n_1,n_2} a_{n_1,n_2'}, \tag{9}$$

and the summation is over even integers and the normalization constant $K_{n_1,n_2}=1$ if $n_1=n_2$ and $=1/2$ if $n_1\neq n_2$. For the purpose of clarity, we have suppressed the state number index n and basis state index j, i.e., $a_{n,j(n_1,n_2)}=a_{n_1,n_2}$. In this case, the y subsystem has been traced out. Similarly another RDM, $\mathbf{R}_y$, with elements $\langle n_2|\rho^{(y)}|n_2'\rangle$ can be obtained by tracing over x variables. Let $\mathbf{A}$ represent the eigenvector matrix of dimension $(m+2)/2$ with elements a_{n_1,n_2}, where $n_1,n_2=0,2,4,\ldots,m$ label the rows and columns, respectively. Then, in matrix notation, the RDM $\mathbf{R}_x=\mathbf{A}^{\mathbf{T}}\mathbf{A}$ is a matrix of dimension $M=(m+2)/2$. Note that due to symmetry of our system, $\mathbf{R}_x=\mathbf{R}_y$. Hence it is sufficient to diagonalize any one of them.

In our case, $m=318$ and we numerically diagonalize the RDM of dimension 160. The eigenvalues of the RDM for a typical delocalized state and a localized state are plotted in Figs. 4(c) and 4(d). In general, the dominant eigenvalues fall exponentially, though with different rates, for both the generic and the typical localized state. Incidentally, this also indicates that the Schmidt decomposition provides a compact representation for the given eigenstate. Earlier such a behavior was noted for coupled standard maps [2]. The first few dominant eigenvalues of the RDM for localized states display (near) degeneracy [see Fig. 4(d)]. This arises as a consequence of (i) the C_{4v} symmetry of the potential due to which the eigenvector matrix is symmetric, i.e., $a_{n_1,n_2}=a_{n_2,n_1}$ and (ii) the localization is exponential in the direction perpendicular to that in which the quanta of excitation is larger [25], i.e., $a_{N,n_2}\propto\exp(-\omega n_2)$, where $\omega>0$ is a constant independent of N.

The origin of near degeneracy can be understood by considering a simple model of a 4×4 symmetric eigenvector matrix,

$$\mathbf{P}=\begin{pmatrix} a_{0,0} & a_{2,0} & a_{N,0} & a_{N+2,0} \\ a_{2,0} & a_{2,2} & a_{N,2} & a_{N+2,2} \\ a_{N,0} & a_{N,2} & a_{N,N} & a_{N+2,N} \\ a_{N+2,0} & a_{N+2,2} & a_{N+2,N} & a_{N+2,N+2} \end{pmatrix}. \tag{10}$$

Here we have only used the one-dimensional quartic oscillator quantum numbers $(0,2,N,N+2)$ because the localized states can be approximately represented by all possible doublets arising from these quantum numbers. For instance, an adiabatic separation with the $(N,0)$ manifold gives a good estimate for the energy of its localized states [25]. The representation gets better as we add more one-dimensional (1D) quantum numbers to the list above. The exponential localization implies that $a_{n_1,n_2}\approx0$ for $n_1\sim n_2$. Further, $a_{n_1,n_2}\approx0$ if $n_1,n_2\ll N$. Thus, elements $a_{N,N}\sim a_{N+2,N}\sim a_{N+2,N+2}\sim a_{0,0}\approx0$. Then, we can identify a block matrix $\mathbf{B}$ with nonzero elements as

$$\mathbf{B}=\begin{pmatrix} a_{N,0} & a_{N+2,0} \\ a_{N,2} & a_{N+2,2} \end{pmatrix}. \tag{11}$$

Then, the eigenvector matrix $\mathbf{P}$ can be approximated as

$$\mathbf{P}\approx\begin{pmatrix} \mathbf{0} & \mathbf{B} \\ \mathbf{B}^T & \mathbf{0} \end{pmatrix}. \tag{12}$$

Under the conditions assumed above, the RDM separates into two blocks which are transpose of one another. Thus, the reduced density matrix will have the form

$$\mathbf{R}=\mathbf{P}^\mathbf{T}\mathbf{P}=\begin{pmatrix} \mathbf{B}\mathbf{B}^\mathbf{T} & \mathbf{0} \\ \mathbf{0} & \mathbf{B}^\mathbf{T}\mathbf{B} \end{pmatrix}. \tag{13}$$

Since the eigenvalues remain invariant under transposition of a matrix, i.e., the eigenvalues of $\mathbf{B}\mathbf{B}^\mathbf{T}$ and $\mathbf{B}^\mathbf{T}\mathbf{B}$ are identical and hence we obtain the degeneracy. Though we use a 4×4 matrix to illustrate the idea, this near degeneracy would arise for any eigenvector matrix of even dimension, if the symmetry and exponential decay conditions are satisfied.

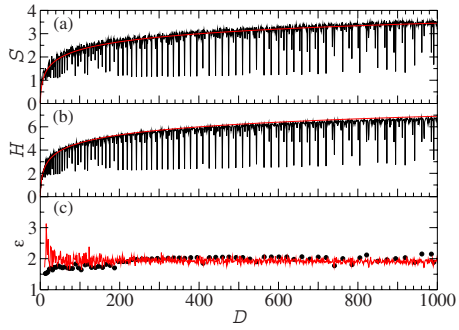

FIG. 5. (Color online) (a) Entanglement entropy, (b) information entropy, and (c) ratio $\varepsilon=H/S$ for the quartic oscillator at $\alpha=30$ from the ground state to the 1000th state. The solid red line in (a) and (b) is the random matrix theory average of entanglement entropy and information entropy, respectively. In (c), the solid line is for the generic delocalized states and filled circles are for the localized states.

For the localized state shown in Fig. 4(b), $N=264$ and the dominant eigenvalue of the RDM using the approximate scheme in Eqs. (10)–(13), is $\lambda_1=0.4434$. This is doubly degenerate and compares favorably with the exact numerical result of 0.4329. As observed in Fig. 4(d), the degeneracy breaks down as we travel down the index. As pointed out, the dominant eigenvalues of the RDM correspond to definite 1D quantum oscillator modes that exhibit exponential decay in the perpendicular mode. This is not true of all the oscillator modes and hence the degeneracy is broken.

C. Entanglement entropy

Entanglement entropy for each eigenstate is computed from the eigenvalues of the RDM using Eq. (4). In Fig. 5(a), we show the entanglement entropy of the quartic oscillator at $\alpha=30$ for 1000 eigenstates starting from the ground state. The entanglement entropy of localized states is much lower than the local average as seen from the dips in the figure. Most of them are much closer to zero and substantiate the fact that they are nearly separable states. In the next section we will show that the entanglement entropy of the localized state is influenced by the bifurcation of the underlying channel periodic orbit.

The generic delocalized states, on the other hand, form the background envelope seen in Fig. 5(a). These chaotic states are not affected by the bifurcations of isolated orbits. It is known that such delocalized states can be modeled using random matrix theory and hence the distribution of their eigenvectors follows Porter-Thomas distribution [29]. The entanglement entropy can also be calculated based on random matrix theory (RMT) assumptions and it is known to be [30] $S_{\mathrm{RMT}}=\ln(\gamma M)$, where $\gamma\approx1/\sqrt{e}$ and M is the dimensionality of the reduced density matrix. In the quartic oscillator case, the Hilbert space is infinite dimensional and we take M to be the effective dimension M_{eff} of the RDM. One indicator of the effective dimension of the state is the inverse participation ratio of the eigenstates. Based on this measure and due to C_{4v} symmetry of the quartic oscillator, we have

$M_{\text{eff}}^2 = D$ where D is the state number. Thus, the effective dimension of RDM is $M_{\text{eff}} = \sqrt{D}$ and we obtain

$$S_{\text{RMT}} = \ln(\gamma M_{\text{eff}}) \sim \ln(\gamma\sqrt{D}). \tag{14}$$

In Fig. 5(a), S_{RMT} is shown as a solid red line and it correctly reproduces the envelope formed by the delocalized states while the localized states stand out as deviations from the RMT based result, namely, S_{RMT}.

While the entanglement entropy is a measure of pure state entanglement, the information (or Shannon) entropy is a measure of eigenstate localization [31] and is defined (for nth eigenstate) as

$$H_n = -\sum_{j=1} |a_{n,j}|^2 \ln|a_{n,j}|^2. \tag{15}$$

In Fig. 5(b), we plot the information entropy for the same set of states as in Fig. 5(a). Comparing the two, we notice that both the entropies are strongly correlated. For the delocalized states, this can be quantitatively seen as follows: The RMT average of information entropy is given by $H_{\text{RMT}} \sim \ln(D/2)$ for large D [32]. The ratio ε between the two entropies is

$$\varepsilon = \frac{H_{\text{RMT}}}{S_{\text{RMT}}} \sim 2\left(\frac{\ln D - \ln 2}{\ln D - 1}\right) \approx 2 \tag{16}$$

for $D \gg 1$. Indeed, in Fig. 5(c) we verify that the ratio $\varepsilon \approx 2$ for all of the generic states (solid red line) except for about the first 50 eigenstates. Even though the ratio ε obtained in Eq. (16) is based purely on RMT results, surprisingly, it also holds good asymptotically for the localized states as well. This is shown as filled circles in Fig. 5(c). Hence, for both the generic and localized states, entanglement is strongly correlated with the degree of eigenstate localization which itself reflects the underlying nature of classical dynamics. In this sense, entanglement is influenced by the nature of classical dynamics. It may be noted that all channel localized states are not localized to the same extent as quantified by their entropies. A close look at the quantum energy spectrum in the vicinity of such localized states reveals the presence of close avoided crossings, i.e., energy differences are less than a mean spacing.

V. ENTANGLEMENT ENTROPY AND BIFURCATIONS

In this section, we show the central result of the paper, viz., that the entanglement entropy attains an extrema in the vicinity of the parameter values at which the underlying periodic orbit undergoes a pitchfork or an antipitchfork bifurcation. As pointed out earlier, the localized states of the quartic oscillator are characterized by the doublet $(N,0)$ and are influenced by the channel periodic orbit. We choose a given localized state, say, with $N=200$ and compute the entanglement of the same state, i.e., (200,0) state as a function of α. The state that can be characterized by the doublet (200,0) will be a localized state at every value of α. All these localized states are in the energy regime of highly excited states where the classical system is predominantly chaotic. The result is shown in Fig. 6(a) as the curve plotted with open circles. The values of α at which the pitchfork and antipitchfork bifurcation takes place is marked in both the horizontal axes of the figure as triangle up and triangle down, respectively. For the purpose of easier visualization, they are connected by vertical lines. Notice that the entanglement entropy attains a local minima in the vicinity of every classical pitchfork bifurcation and it attains a local maxima near every antipitchfork bifurcation. As Fig. 6(a) shows, a similar result is obtained for two different series of localized states ($N=210,0$) and ($N=240,0$). The energies of these states are quite different. The information entropy shown in Fig. 6(b), for the same set of localized states as in Fig. 6(a), is seen to be strongly correlated with the entanglement entropy.

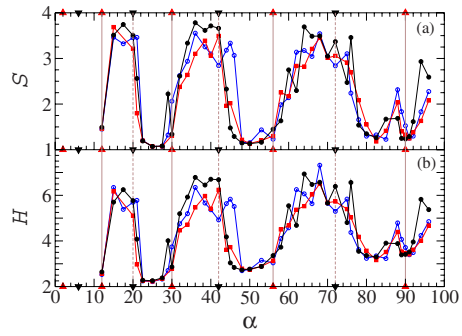

FIG. 6. (Color online) (a) Entanglement entropy and (b) information entropy as a function of α. The three curves correspond to different $(N,0)$-type localized states; solid circles (240,0), open circles (200,0), and squares (210,0). The positions of pitchfork bifurcations (triangle up) and antipitchfork bifurcations (triangle down) are marked on all of the x axes.

At a pitchfork bifurcation, as shown in Fig. 2, the elliptic fixed point corresponding to the channel periodic orbit loses stability and becomes a hyperbolic point. The central elliptic island seen in Fig. 2(a), breaks up into two islands. The localized state that mainly derives its support from the classical structures surrounding the stable fixed point suffers some degree of delocalization, but is largely supported by the stable regions. At an antipitchfork bifurcation, the hyperbolic point becomes an elliptic fixed point and the orbit gains stability and a small elliptic island just comes into existence. Hence, the eigenstate is still largely delocalized since the small elliptic island is insufficient to support it. This heuristic picture is quite sufficient to explain oscillations in localization measures and surprisingly holds well even for the somewhat less intuitive measure of entanglement. Notice that in Fig. 6(a) the extrema in entanglement does not precisely coincide with the bifurcation points. This can be understood as follows. Strictly, if the channel orbit [seen as fixed point $y=0$, $p_y=0$ in Fig. 2(a)] undergoes only this series of pitchfork and antipitchfork bifurcations and nothing else, then this alone would determine the extent of eigenstate localization, and we can expect the extrema in entanglement to coincide with such bifurcation points. However, it is known that the localized state is supported by the classical phase space structure surrounding the fixed point and not just the fixed point alone. The Poincaré section of the quartic oscillator shows that this elliptic region that supports the eigenstate has other resonances as well. These display different patterns of bifurcation and stability properties [33]; for instance, the

period-4 orbit shown in Fig. 2(a) that winds around the channel orbit. Eigenstate (de)localization and hence entanglement too is correlated with the nature of classical dynamics in the vicinity of channel orbit and this also includes other orbits in this region. In view of this, as seen in Fig. 6(a), the extrema in entanglement do not coincide with the bifurcation points but are seen to be shifted slightly and correlated with the degree of localization. This is only to be expected even from general considerations since any quantum-classical correspondence is exact only for the harmonic oscillator and is approximate for coupled anharmonic oscillator systems.

The striking similarity between the classical stability curve for a particular periodic orbit, namely the channel orbit, in Fig. 3 and the variation of the entanglement of the localized state is to be noted. However, both the curves cannot be put on top of one another since they are not of the same frequency. For every two extrema in a stability curve there are four extrema in entanglement. We have also numerically verified (not shown here) that a similar result is obtained in the case of another potential where pitchfork and antipitchfork bifurcations of the channel periodic orbit play an important role, namely, in the potential $V(x,y)=x^2+y^2+\beta x^2y^2$, where β is the chaos parameter. Oscillations in the information entropy with a scaled chaos parameter similar to that in Fig. 6(b) was reported earlier in Ref. [25]. A calculation of the von Neumman entropy shows that it too has the same oscillations as in Fig. 6(a). This is consistent with the notion that the larger the delocalization, the larger is the entanglement entropy since at points of the pitchfork bifurcations there is relative delocalization. There is evidence to suggest that this is a general trend. For instance, for the case of the Ising model in external magnetic fields a direct correlation between the participation ratio of the states and measures of multipartite entanglement has been reported [34]. In the context of disordered Heisenberg models a recent study [35] comprehensively explores this correlation.

It was noted earlier that when the corresponding classical system undergoes a pitchfork bifurcation, the entanglement entropy defined by Eq. (4) attains a maximum [11], and this was conjectured to be a generic property. We note that this, apparently contradictory result, is however in the context of an equilibrium point undergoing a bifurcation and the relevant state is the ground state. In the case considered in the present work the orbit that is bifurcating is a periodic orbit and the states are all highly excited. In this situation there is a much tighter correlation between more conventional measures of localization (Shannon entropy, participation ratio, etc.) and entanglement. We also mention (results not shown here) that for the quartic oscillator in Eq. (5), the ground state entanglement increases monotonically with the chaos parameter and does not show any of the oscillations displayed in Fig. 6. The quantum effects dominate the ground states. Hence, the effect of bifurcations on them can be different from the states in the semiclassical region.

Finally we comment on the entanglement at $\alpha=0$. This is a separable case and it is straightforward to show that entanglement entropy S at $\alpha=0$ is ln 2. This is because we are considering parity symmetric states and at $\alpha=0$ there is a degeneracy allowing us to choose for eigenfunctions an infinite set with unequal entanglements, in the range $(0,\ln 2)$. For instance, the eigenstate $[\phi_{n_1}(x)\phi_{n_2}(y)+\phi_{n_2}(x)\phi_{n_1}(y)]$ has $S=\ln 2$ but $\phi_{n_1}(x)\phi_{n_2}(y)$ is also a valid eigenstate with $S=0$. Our basis set corresponds to the former choice and hence we obtain $S=0.693\sim\ln 2$ in our simulations. This is irrelevant for $\alpha\neq 0$ because the eigenstates are nondegenerate and unique.

As the parameter α is increased, the quartic oscillator gets to be predominantly chaotic and this should imply an increase in entanglement. However, this is true only for the generic delocalized states as seen in Fig. 5. The localized states are influenced not so much by the increasing volume of the chaotic sea but by the specific periodic orbits that underlie them. Hence, for these states, it is only to be expected that the qualitative changes in the phase space in the vicinity of the corresponding periodic orbits affect quantum eigenstates and their entanglement as well. This can be expected to be a generic feature of entanglement in quantum eigenstates of mixed systems.

VI. CONCLUSIONS

In summary, we have considered a smooth Hamiltonian system, namely the two-dimensional coupled quartic oscillator, as a bipartite system. The coupled quartic oscillator is a classically chaotic system. One particular class of eigenstates of this system, namely, the localized states, are strongly scarred by the channel periodic orbits. We consider the effect of bifurcations of the channel orbit on the entanglement of the quantum eigenstates scarred by it. We have shown that the entanglement entropy of these localized states is influenced by the bifurcations in the underlying channel periodic orbit. When this orbit undergoes a pitchfork bifurcation, the entanglement is nearly a local minimum and when it undergoes an antipitchfork bifurcation the entanglement is almost a local maximum. Physically, this is related to the presence or the absence of elliptic islands in the phase space in the vicinity of the channel orbit. We expect this to be a general feature of bipartite quantum systems whose classical analog display bifurcations.

ACKNOWLEDGMENTS

This work was partially supported by the U.S. National Science Foundation through a grant for the Institute for Theoretical Atomic, Molecular and Optical Physics at Harvard University and Smithsonian Astrophysical Observatory, where one of the authors (V.B.S.) visited during 2006. The authors thank J. N. Bandyopadhyay for discussions and comments. The authors acknowledge the comments and queries of an anonymous referee which helped to improve the paper.

[1] M. A. Nielsen and I. L. Chuang, *Quantum Computation and Quantum Information* (Cambridge University Press, Cambridge, 2000).
[2] A. Lakshminarayan, Phys. Rev. E **64**, 036207 (2001); K. Furuya, M. C. Nemes, and G. Q. Pellegrino, Phys. Rev. Lett. **80**, 5524 (1998); P. A. Miller and S. Sarkar, Phys. Rev. E **60**, 1542 (1999); X. Wang, Shohini Ghose, Barry C. Sanders, and Bambi Hu, *ibid.* **70**, 016217 (2004); C. Mejia-Monasterio, G. Benenti, G. G. Carlo, and G. Casati, Phys. Rev. A **71**, 062324 (2005); Ph. Jacquod, Phys. Rev. Lett. **92**, 150403 (2004); C. Petitjean and Ph. Jacquod, *ibid.* **97**, 194103 (2006).
[3] H. Fujisaki, T. Miyadera, and A. Tanaka, Phys. Rev. E **67**, 066201 (2003); J. N. Bandyopadhyay and A. Lakshminarayan, *ibid.* **69**, 016201 (2004).
[4] A. J. Scott and C. M. Caves, J. Phys. A **36**, 9553 (2003).
[5] Xi-Wen Hou and Bambi Hu, Phys. Rev. A **69**, 042110 (2004).
[6] Marcel Novaes and Marcus A. M. de Aguiar, Phys. Rev. E **70**, 045201(R) (2004).
[7] Q. Xie and W. Hai, Eur. Phys. J. D **33**, 265 (2005).
[8] R. M. Angelo, K. Furuya, M. C. Nemes, and G. Q. Pellegrino, Phys. Rev. A **64**, 043801 (2001).
[9] S. Schneider and G. J. Milburn, Phys. Rev. A **65**, 042107 (2002).
[10] M. C. Nemes *et al.*, Phys. Lett. A **354**, 60 (2006).
[11] A. P. Hines, R. H. McKenzie, and G. J. Milburn, Phys. Rev. A **71**, 042303 (2005).
[12] A. P. Hines, C. M. Dawson, R. H. McKenzie, and G. J. Milburn, Phys. Rev. A **70**, 022303 (2004).
[13] Q. Xie and W. Hai, Eur. Phys. J. D **39**, 277 (2006).
[14] H. Friedrich and D. Wintgen, Phys. Rep. **183**, 37 (1989).
[15] J.-M. Mao and J. B. Delos, Phys. Rev. A **45**, 1746 (1992).
[16] A. Lakshminarayan and V. Subrahmanyam, Phys. Rev. A **67**, 052304 (2003).
[17] H. Li, X. Wang, and B. Hu, J. Phys. A **37**, 10665 (2004).
[18] H. Li and X. Wang, Mod. Phys. Lett. B **19**, 517 (2005).
[19] O. Bohigas, S. Tomsovic, and D. Ullmo, Phys. Rep. **233**, 45 (1993).
[20] W.-H. Steeb, J. A. Louw, and C. M. Villet, Phys. Rev. D **33**, 1174 (1986); A. Carnegie and I. C. Percival, J. Phys. A **17**, 801 (1984).
[21] K. M. Atkins and G. S. Ezra, Phys. Rev. A **50**, 93 (1994).
[22] B. Eckhardt, G. Hose, and E. Pollak, Phys. Rev. A **39**, 3776 (1989); J. Zakrzewski and R. Marcinek, *ibid.* **42**, 7172 (1990).
[23] K. Muller and D. Wintgen, J. Phys. B **27**, 2693 (1994); D. Delande and J. C. Gay, Phys. Rev. Lett. **59**, 1809 (1987).
[24] H. Yoshida, Celest. Mech. **31**, 363 (1983); Physica D **29**, 128 (1987).
[25] M. S. Santhanam, V. B. Sheorey, and A. Lakshminarayan, Phys. Rev. E **57**, 345 (1998).
[26] M. V. Berry, Philos. Trans. R. Soc. London, Ser. A **287**, 237 (1977); J. Phys. A **10**, 2083 (1977).
[27] E. J. Heller, Phys. Rev. Lett. **53**, 1515 (1984); in *Les Houches LII, Chaos and Quantum Physics*, edited by M.-J. Giannoni, A. Voros, and J. Zinn-Justin (North-Holland, Amsterdam, 1991).
[28] M. V. Berry, Proc. R. Soc. London, Ser. A **423**, 219 (1989); E. B. Bogomolny, Physica D **31**, 169 (1988).
[29] F. Haake, *Quantum Signatures of Chaos* (Springer-Verlag, Berlin, 2000).
[30] J. N. Bandyopadhyay and A. Lakshminarayan, Phys. Rev. Lett. **89**, 060402 (2002).
[31] F. Izrailev, Phys. Rep. **196**, 299 (1990).
[32] K. Zyczkowski, J. Phys. A **23**, 4427 (1990).
[33] M. Brack, M. Mehta, and K. Tanaka, J. Phys. A **34**, 8199 (2001); M. Brack, S. N. Fedotkin, A. G. Magner, and M. Mehta, *ibid.* **36**, 1095 (2003).
[34] J. Karthik, Auditya Sharma, and Arul Lakshminarayan, Phys. Rev. A **75**, 022304 (2007).
[35] Winton G. Brown, Lea F. Santos, David J. Starling, Lorenza Viola, e-print arXiv:0707.1331.